15.5 The effects of varying low-level, environmental stability on low-level rotation in numerical simulations of elevated supercells

CHRISTOPHER J. NOWOTARSKI* AND PAUL MARKOWSKI

Department of Meteorology, The Pennsylvania State University, University Park, Pennsylvania

1. Introduction and motivation

There is considerable anecdotal evidence that supercell thunderstorms are sensitive to changes in the environmental low-level static stability and convective inhibition (CIN). For example, "elevated" supercells are widely assumed to pose a greatly diminished tornado threat compared to "surface-based" supercells. [An elevated storm is defined herein as one that draws its inflow from a layer not in contact with the surface in close proximity to the storm (Colman 1989).] Boundary layers which may be characterized by relatively large surface-based CIN include both nocturnal boundary layers as well as the air mass which resides on the cool side of a thermal boundary (e.g., an outflow boundary or front).

Our ongoing research is geared toward answering the following question: "Why are elevated supercells less likely to produce tornadoes than surface-based supercells?" The work reported herein uses idealized numerical simulations with a horizontally homogeneous environment. Thus, at this early stage, we are effectively studying the (presumably) simpler case of a supercell occurring in a nocturnal boundary layer rather than the case of a supercell encountering horizontal heterogeneity in the form of a preexisting outflow boundary.

A major nowcasting challenge in the case of a storm crossing a thermal boundary is that the low-level vertical wind shear is typically enhanced on the immediate cool side of the boundary. Thus, there are potentially competing effects, in that the increased CIN tends to be detrimental to low-level rotation, whereas the increased low-level shear tends to favor low-level rotation. For example, Maddox et al. (1980), Markowski et al. (1998), and Rasmussen et al. (2000) documented a significant number of tornadoes within supercells shortly after the storms crossed thermal boundaries, and numerical simulations by Atkins et al. (1999) further supported the notion that horizontal vorticity enhancements along such boundaries are important. On the other hand, Markowski et al. (1998) and Doswell et al. (2002) have documented supercells that were tornadic or had rapid intensifications of low-level rotation while interacting with a thermal boundary, but then became elevated and nontornadic after crossing the boundary into air masses characterized by substantial surface-based CIN. Similar competing effects are commonly observed when nocturnal boundary layers form, as the low-level stabilization tends to be accompanied by the development of a nocturnal low-level wind maximum and an increase in low-level shear. Developing an understanding of the dynamics that suppress low-level rotation in our simplified numerical experiments is a first step toward improving our ability to anticipate how a storm will respond to the static stability and vertical wind shear modulations associated with nocturnal cooling or a boundary-crossing.

As stated above, this extended abstract summarizes the results of idealized, three-dimensional numerical simulations of elevated supercells initialized with horizontally homogeneous environments having surface-based CIN. These elevated supercells are compared to a supercell in a control experiment, which was initialized in an environment without low-level static stability. The goal is to identify the dynamics responsible for the suppression of low-level rotation in the elevated supercells. The simulations are designed to (1) investigate the parameter space of the surface temperature deficit and stable layer depth as well as to (2) determine if the suppression of near-ground vertical vorticity in elevated storms owes to a lack of near-ground circulation as a result of downdrafts being less able to penetrate the stable air mass [downdrafts are the only means by which vertical vorticity can develop at the surface in a horizontally homogeneous environment without a Coriolis effect (e.g., Davies-Jones and Brooks 1993)], inhibited convergence of near-ground circulation as a result of weaker vertical velocities, or a combination of both effects.

The configuration of the model and initial conditions are further discussed in section 2. Section 3 presents the results of the parameter space investigation. In section 4, the control supercell is more closely compared to an archetypical elevated supercell in order to investigate the dynamics responsible for the differences between the two simulations. Section 5 contains final remarks.

2. Numerical model and initial conditions

The numerical simulations are performed using the Bryan Cloud Model, Version 1, Release 11 (Bryan 2002). The model domain is 80 km x 80 km x 20 km with a horizontal grid spacing of 500 m. The vertical grid is stretched; the vertical grid spacing is 50 m below 1 km (the lowest grid level is at 25 m) and increases to 500 m above 12 km. Each simulation is run for 7200 s. A large (small) time step of 3 s (0.5 s) is used. Open, wave-radiating boundary conditions are employed at the lateral boundaries; the upper and lower boundaries are free-slip. Beneath the upper boundary there also is a Rayleigh-damping sponge layer.

All of the storms are triggered by a warm bubble having a horizontal radius of 10 km and a vertical radius of 1.5 km. The control simulation is initialized with a horizontally homo-

**Corresponding author address*: Christopher Nowotarski, Department of Meteorology, Pennsylvania State University, 503 Walker Building, University Park, PA 16802; *e-mail*: cjn5012@psu.edu.

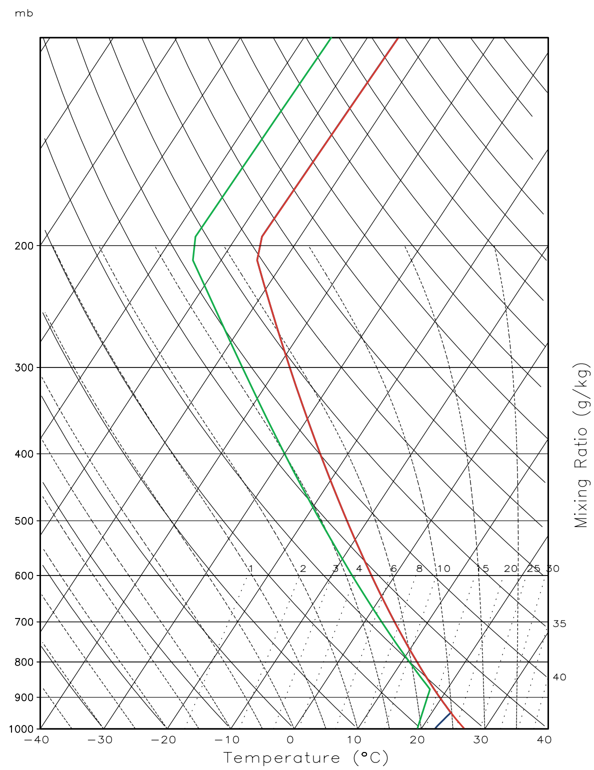

FIG. 1. The analytic sounding (Weisman and Klemp 1982) used in each simulation. Mixing ratio is shown in green, whereas temperature in the control simulation is shown in red. Near the surface, an example stable boundary layer (500 m deep with a temperature deficit of 5°C) is shown in blue. The charateristics of this inversion are altered in each elevated simulation.

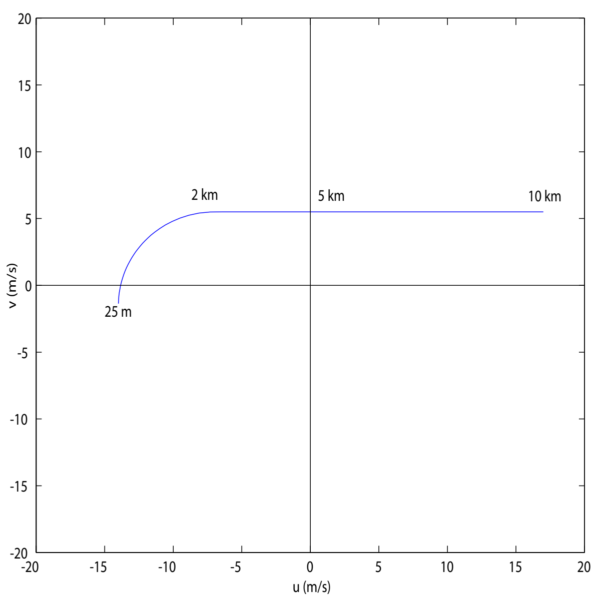

FIG. 2. The idealized, clockwise-turning hodograph used as the initial vertical wind profile for each simulation (Rotunno and Klemp 1982) with various heights labeled.

geneous environment using the analytic sounding of Weisman and Klemp (1982) with a water vapor mixing ratio of 14 g kg^{-1} at the surface. This sounding has a CAPE of approximately 2500 J kg^{-1} and a lifting condensation level of approximately 1200 m. In each subsequent experiment, this temperature profile is modified by the addition of a stable surface layer (Fig. 1) with no change to the sounding above the stable layer. The imposed stable layers have a constant lapse rate that depends on the surface temperature and stable layer depth. The stable layer depths range from 100 m to 1 km and the surface temperature deficit relative to the control sounding varies from 2.5°C to 10°C. Where the introduction of a stable layer results in supersaturation the environmental relative humidity is reduced to 95%.

The clockwise-turning hodograph used by Rotunno and Klemp (1982; our Fig. 2) is used in all of the experiments, though straight and semicircular hodographs were used in sensitivity tests. Although splitting storms develop, our focus is on the dominant right-moving (cyclonically rotating) supercell that results in each of the simulations.

3. General relationship between elevated supercell characteristics and the low-level temperature profile

The control supercell and elevated supercells are compared at 5100 s (85 minutes) (Figs. 3 and 4), the time at which the control supercell displays its maximum near-ground vertical vorticity. Horizontal cross-sections of vertical vorticity and vertical velocity were analyzed near the ground (25 m and 125 m for vertical vorticity and vertical velocity, respectively) and at midlevels (4 km). The risk in performing comparisons at a common time is that storms may evolve at different rates, such that differences among storms observed at a common time may not reflect fundamental dynamical differences among the storms as much as simply differences in the time at which certain aspects of the storm develop [e.g., there is some risk that an elevated storm differing considerably from the control storm at 5100 s could look very similar to the control storm (at 5100 s) 10-20 minutes later]. Thus, there might be advantages to comparing storms at a common evolutionary milestone instead, e.g., the time of maximum vertical vorticity at some level. The possible downside of this latter approach, however, is that differences in how the storms arrive at the evolutionary milestone might be masked. In our ongoing investigation, simulated storms were compared both at common times as well as common evolutionary milestones (time of maximum vertical vorticity). It was found that the differences among the numerical experiments were largely insensitive to whether the comparisons were made at a common time or common evolutionary milestone.

We are somewhat casually referring to all of the supercells initiated in environments having a stable lower atmosphere as “elevated” supercells; however, in the case of very shallow stable layers with a surface temperature deficit that is relatively small (e.g., a 100 m stable layer with a surface temperature deficit of only 2.5°C), it was found that the supercells were able to lift surface air to the level of free convection via a strong dynamic vertical pressure gradient. Thus, despite the enhanced surface-based CIN relative to the control, some of the supercells simulated in environments having shallow stable layers were not strictly “elevated.” It is obviously of great operational interest how much CIN a supercell can encounter and still be “surface-based.” This issue is beyond the scope of the present paper and is almost certainly not easily generalized because the dynamic pressure field of a supercell likely varies significantly from one storm to another.

Near-ground vertical vorticity and low-level updraft speed within the simulated storms generally decrease with increasing CIN (Figs. 3 and 5). A strong negative correlation (linear correlation coefficient of -0.85) exists between CIN and the maximum vertical vorticity at 25 m (Fig. 5a). For a given stable lapse rate, near-ground mesocyclones generally weaken as the surface temperature in the environment is cooled, and for a given environmental surface temperature that is cold relative to the control, near-ground mesocyclones generally weaken as the depth of the stable layer increases. Furthermore, there is a moderate negative correlation (coefficient of -0.57) between CIN and maximum updraft speed at low levels (Fig. 5c) with a 40% decrease from the control updraft to the weakest updraft. In every stable layer simulation, the resulting supercell exhibits weaker vertical vorticity and a weaker updraft at low levels than in the control simulation. Even stable layers that are very shallow (100 m) and only marginally resolved yield supercells with near-ground mesocyclones that are noticeably weaker than in the control supercell.

There is relatively little variation in midlevel vertical vorticity and vertical velocity as a function of CIN (Figs. 4 and 5). CIN and vertical vorticity are not well-correlated at midlevels (Fig. 5b) whereas CIN and maximum midlevel updraft speed have a moderate negative correlation (coefficient of -0.60). However, updraft speed decreases by only 15% between the strongest and weakest updrafts. The simulation initialized with the deepest and coldest stable layer yields the storm with the weakest midlevel (and low-level) updraft speed and vertical vorticity, but the midlevel vertical vorticity decrease is negligible relative to the control supercell (less than 1.6 x 10-3 s-1 weaker), as is the midlevel updraft speed (only 2.5 m s^{-1} weaker). In summary, the strength of midlevel rotation in the simulated elevated supercells is largely unaffected by the low-level stable layers, and the strength of the midlevel updraft is only marginally affected.

Finally, with respect to downdrafts, although maximum downdraft speeds are relatively similar at both low levels and midlevels in the control and stable-layer simulations at 5100 s, maximum downdraft speeds at low levels are generally stronger in the control simulation than in stable-layer simulations. The weaker downdrafts in the stable-layer simulations are a result of air parcels having reduced negative buoyancy as they descend through the shallow stable (cool) layers (not shown).

4. Comparison of the control supercell with the archetypical elevated supercell

The dynamics responsible for the suppression of near-ground rotation in the elevated supercells are best understood through a more detailed comparison of the control simulation with an archetypical elevated supercell simulation. Below we investigate the dynamical differences between the control supercell and, without loss of generality, the elevated supercell that develops within the environment initialized with a 500 m-deep stable layer with a surface temperature deficit of 5°C.

Vertical vorticity time series (Fig. 6) reveal that rotation is nearly always stronger in the control supercell near the surface, whereas at midlevels neither storm displays consistently stronger rotation than the other, in agreement with the finding in section 3 that near-ground vertical vorticity decreases as CIN increases, and midlevel vertical vorticity is largely insensitive to CIN. Furthermore, time series of maximum vertical velocity (Fig. 7) suggest a similar relationship between CIN and updraft strength at low- and midlevels.

On average, the low-level downdrafts are stronger in the control supercell than in the elevated supercell, but at midlevels, the average downdrafts are of comparable strength (Fig. 8). At two times when the near-ground vertical vorticity is significantly weaker in the stable-layer case than in the control case, 60 minutes and 85 minutes, there is relatively little difference in low-level or midlevel downdraft strength. However, immediately prior to these times the control storm has a significantly stronger downdraft at low levels. At midlevels, the downdraft is stronger in the control directly prior to 85 minutes but similar in strength to the stable-layer simulation directly prior to 60 minutes.

In order to better understand the dynamical reasons for why the control supercell contains a stronger near-ground mesocyclone than the elevated supercell, we examine the evolution of material circuits (and the circulation about those circuits) in each storm, traced backward from the near-ground mesocyclone, following the approach of Rotunno and Klemp (1985). The material circuits are initiated at a height of 50 m above ground level and surround the near-ground vertical vorticity maxima at 85 minutes. The circuits are 4 km in diameter and are stepped backwards 20 minutes in time using a 4th-order Runge-Kutta trajectory algorithm.

The evolution of the material circuit in our control simulation is similar to the evolution in the simulation of Rotunno and Klemp. As the circuit advances forward in time, it converges around the near-ground vertical vorticity maximum (Fig. 9). A section of the curve descends from 150 m above ground level, whereas the rest of the curve approaches relatively horizontally with the storm inflow (Fig. 10). Generation of circulation is proportional to the projection of the circuit onto a vertical plane that intersects buoyancy isopleths. This mechanism leads to an increase in circulation around the circuit with time (Fig. 11).

In the elevated supercell, less circulation is generated along a material circuit. Static stability limits the ability of the downdraft to reach low levels, thus preventing downward excursions of the material circuit. Consequently, the predominately horizontal orientation of the material circuit decreases the amount of circulation generated along the curve. The horizontal buoyancy gradient is also weaker across the material curve, further contributing to less circulation generation.

These results were also qualitatively similar in the case of both semicircular and straight hodographs. In each case, weaker low-level mesocyclones were observed in the elevated supercell due to weaker generation and convergence of circu-

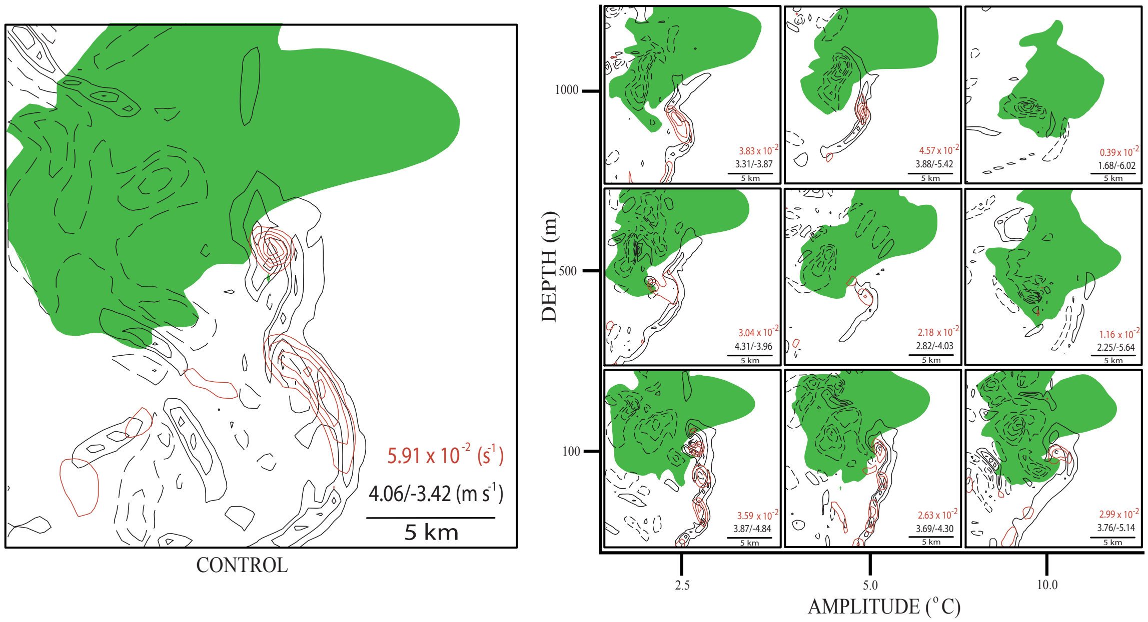

FIG. 3. Low-level, horizontal cross-sections of the control (left) and stable-layer (right) simulations at 5100 s (85 minutes). Stable-layer simulations are organized with depth as the ordinate and surface temperature deficit (amplitude) as the abcissa. Green shaded regions represent rainwater mixing ratio > 1 g kg^{-1} at 125 m AGL. Updraft(downdraft) velocity is contoured in solid(dashed) black at intervals of 1 m s^{-1}. Vertical vorticity is contoured in red at 25 m AGL in 0.01 s^{-1} intervals. Maximum values of vertical vorticty and updraft/downdraft velocity within the horizontal domain are reported in the lower right corner of each cross-section.

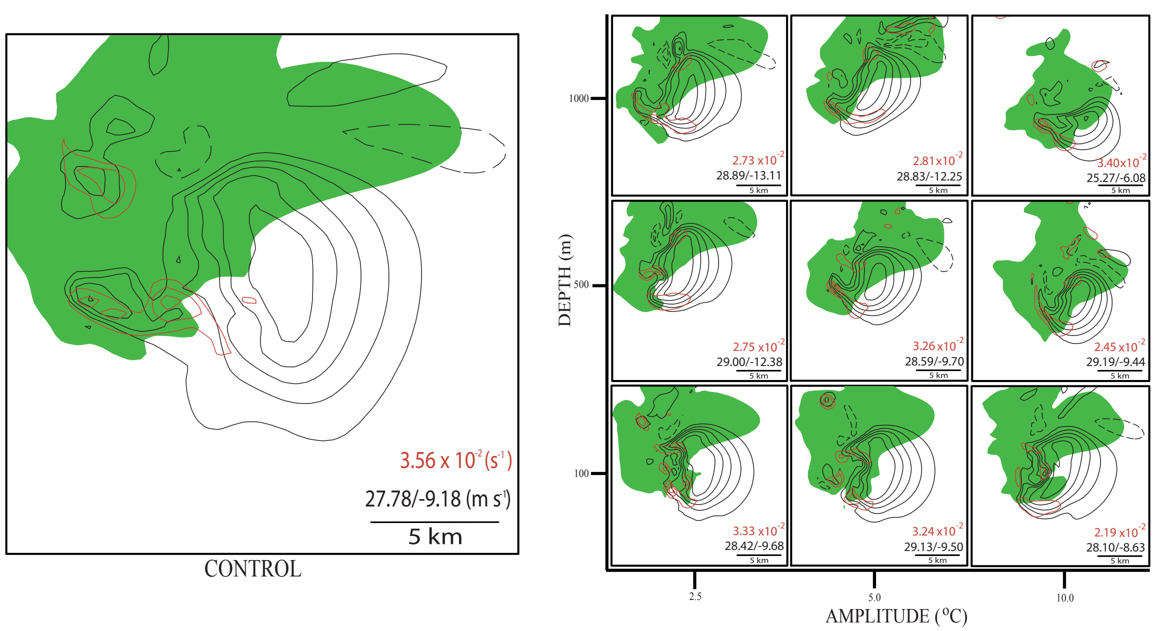

FIG. 4. Midlevel, horizontal cross-sections of the control (left) and stable-layer (right) simulations at 5100 s (85 minutes). Same as in Fig. 3 but vertical vorticity and vertical velocity cross-sections are 4 km AGL. Vertical velocity contours are at 5 m s^{-1}.

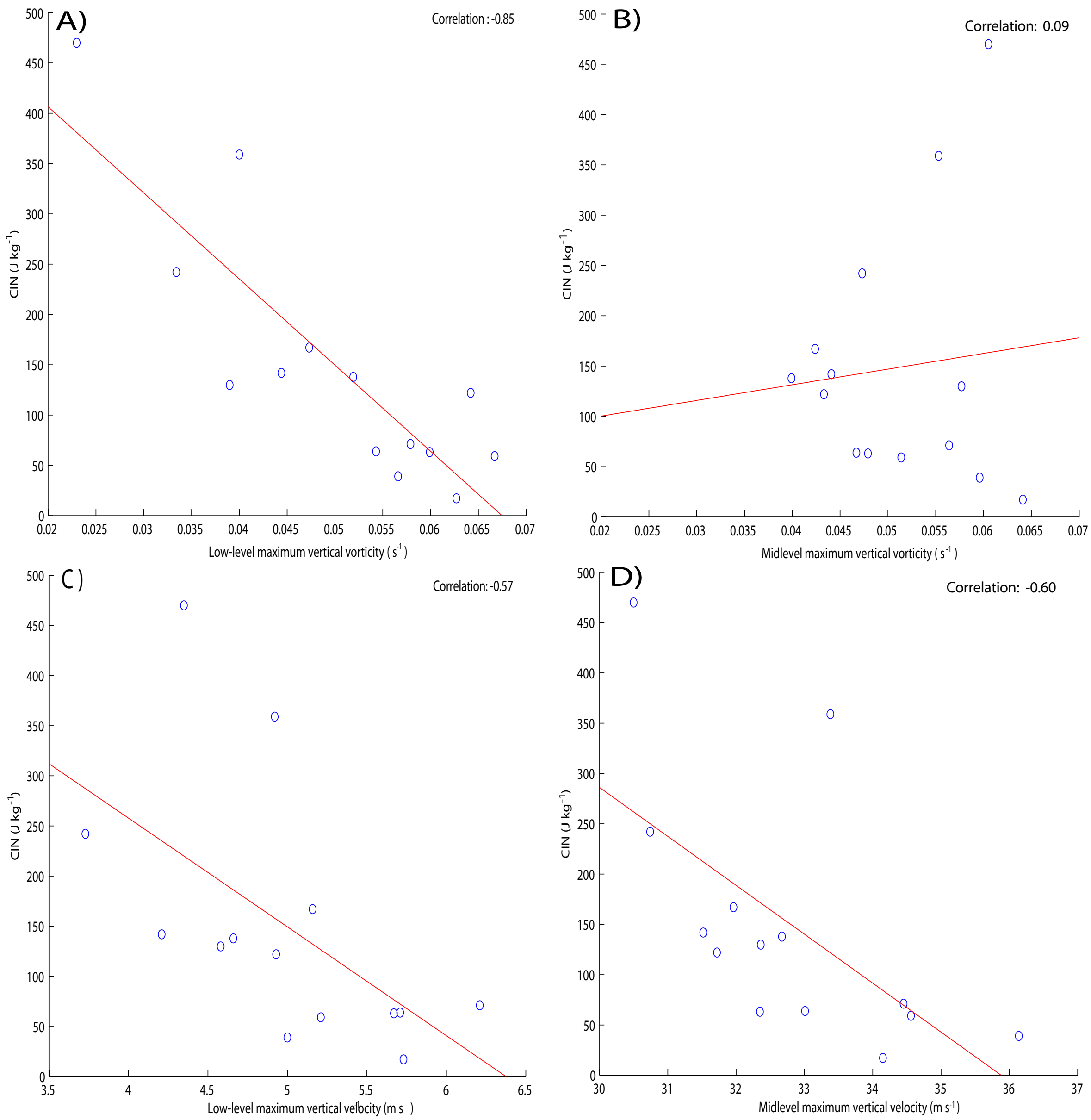

FIG. 5. Graphs of CIN vs. maximum a) low-level vertical vorticity, b) midlevel vertical vorticity, c) low-level vertical velocity, and d) midlevel vertical velocity for a range of varying stable-layer simulations (some are included that are not shown in Figs. 3 and 4). A linear trendline and correlation coefficient are also included.

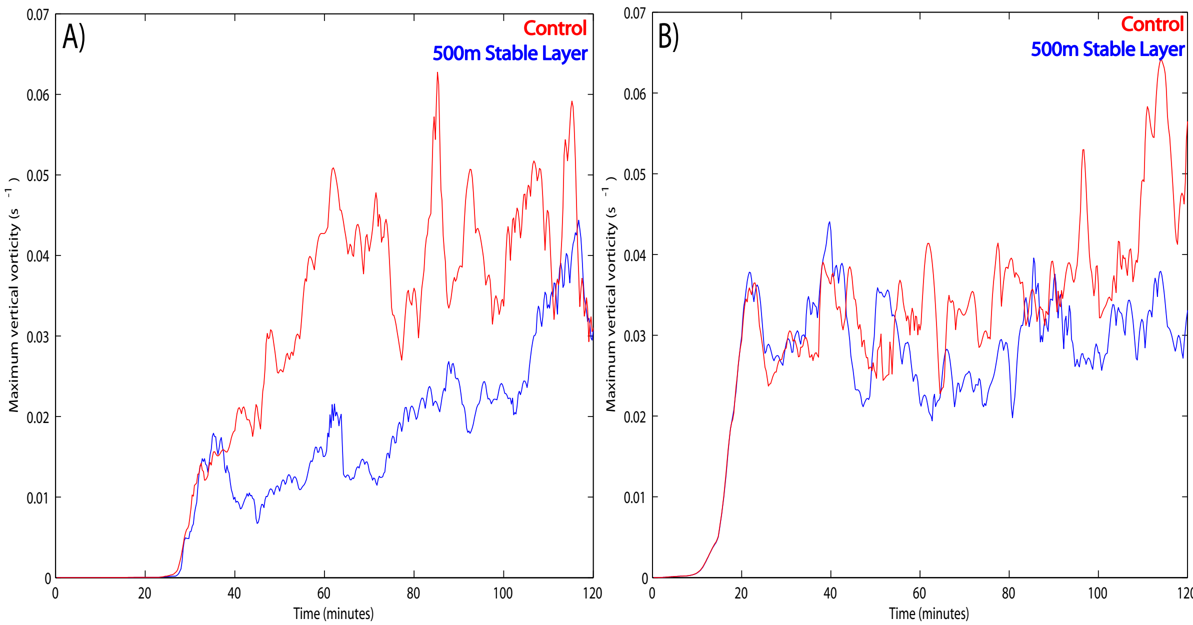

FIG. 6. Time series of maximum vertical vorticity at a) low-levels and b) midlevels in the right-moving supercell for the control (red) and 500 m deep, 5°C surface temperature deficit stable-layer (blue) simulations.

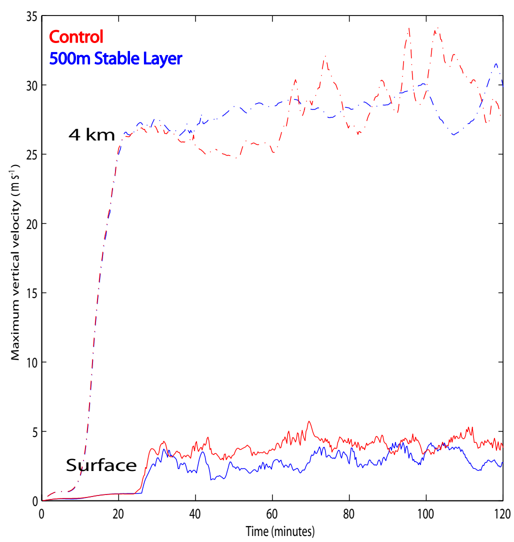

FIG. 7. Time series of maximum vertical velocity (updraft speed) at low-levels (solid lines) and midlevels (dashed lines) in the right-moving supercell for the control (red) and 500 m deep, 5°C surface temperature deficit stable-layer (blue) simulations.

lation. Therefore, we are confident that such findings are not limited to a single wind profile.

5. Summary and conclusions

The addition of a low-level statically stable layer, similar to a nocturnal boundary layer or mesoscale cold pool, decreases both the low-level rotation and low-level vertical velocities in simulated supercell thunderstorms. Midlevel storm characteristics are much less sensitive to the changes in low-level stability, at least for the range of conditions explored herein.

A closer comparison of the control supercell with an archetypical elevated supercell found considerably weaker downdrafts at low levels in the elevated supercell, especially in the periods leading up to the times at which the differences between the vertical vorticity in the elevated and control supercell simulations were greatest. The weaker downdrafts in the elevated supercell case are the result of reduced negative buoyancy, i.e., a smaller density difference between the descending parcels and the relatively cool environmental air within the prescribed low-level stable layer. The smaller downward excursions associated with the weaker downdrafts coupled with a weaker horizontal buoyancy gradient limit the circulation about the material circuit that is converged in the process of near-ground vertical vorticity amplification. Not only is the near-ground circulation weaker in the elevated supercell, but the low-level updraft is weaker as well, thereby also contributing to the suppressed vertical vorticity amplification.

It is probable that more variables than simply the thermodynamic characteristics of a stable layer are important to the development of low-level rotation in elevated supercells. Other factors like wind shear and moisture are outside the scope of this initial study. Furthermore, these simplified simulations are conducted in a horizontally homogenous environment, whereas it has been found that storm interactions with (horizontally

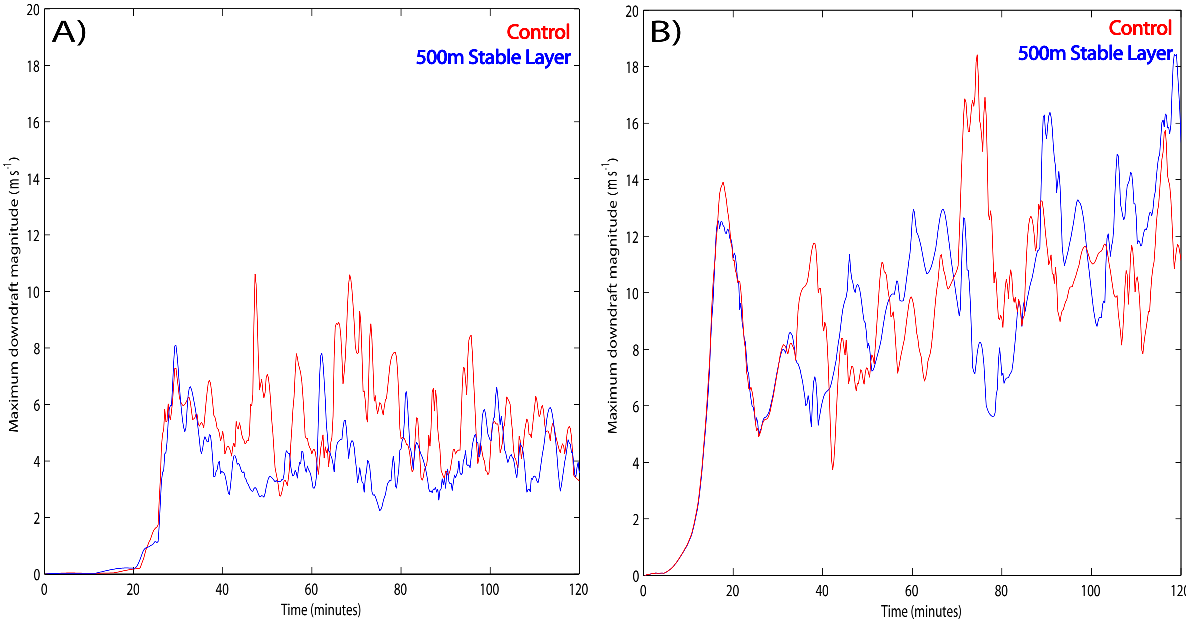

FIG. 8. Time series of maximum downdraft magnitude at a) low-levels and b) midlevels in the right-moving supercell for the control (red) and 500 m deep, 5°C surface temperature deficit stable-layer (blue) simulations.

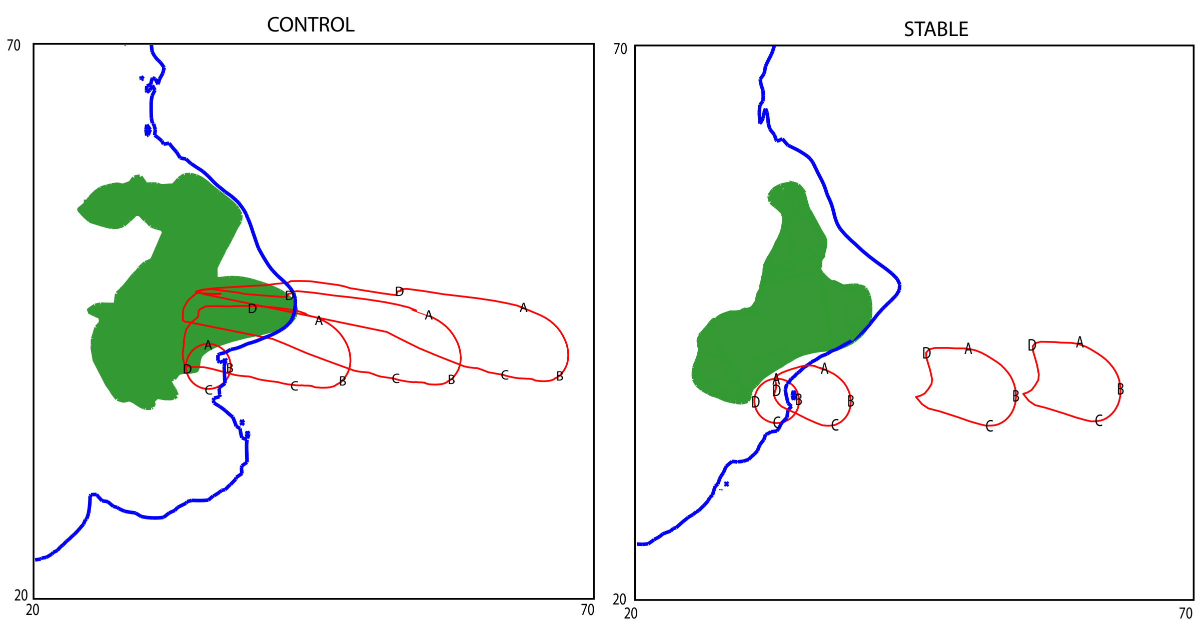

FIG. 9. Overhead view showing location of material circuit (red) at 85 min, the time of maximum circulation generation in each simulation, 75 minutes, and 70 minutes for the control (left) and 500 m deep, 5°C surface temperature deficit stable-layer (right) simulations. Four air parcels (A-D) are labeled on each curve and rainwater mixing ratio > 1 g kg^{-1} at 125 m AGL is shaded green.

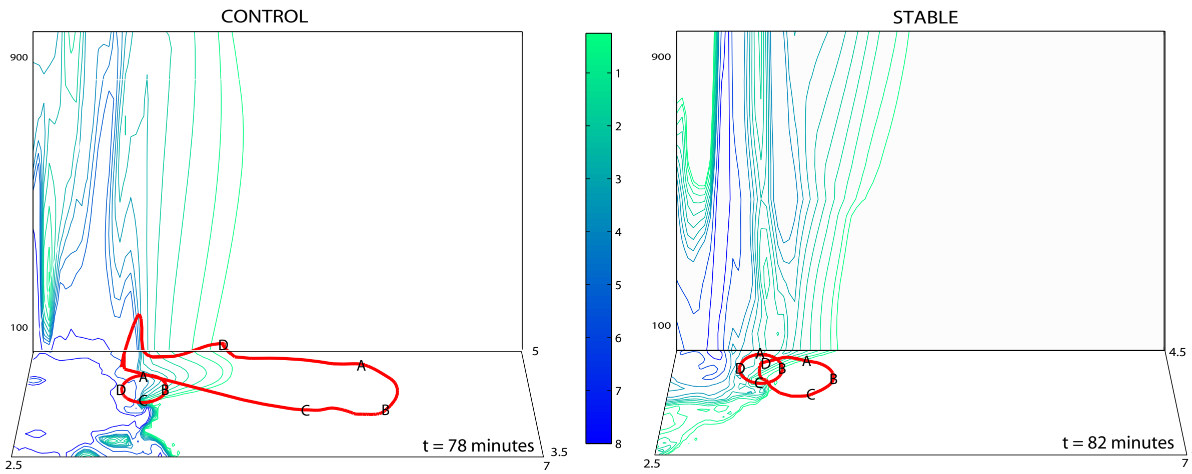

FIG. 10. Perspective comparison, looking North, of material circuits (red) in control (left) and stable-layer (right) simulations at the time of greatest circulation generation in each case. $\theta\rho$' (a proxy for buoyancy that is chosen because it accounts for moisture and hydrometeor loading) is contoured both horizontally at the surface and vertically in the y-z plane where each material circuit is most vertically oriented. Contours of $\theta\rho$' [-K] are at uneven intervals, but valued according to the colorbar. The horizontal axes are labeled in kilometers whereas the vertical axis is labeled in meters.

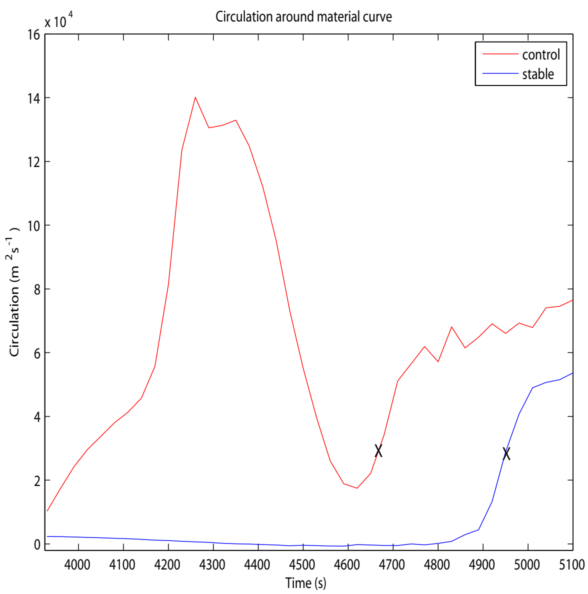

FIG. 11. Time series of circulation in both the control (red) and 500 m deep, 5°C surface temperature deficit stable-layer (blue) simulations. The time of each material circuit used in Fig. 10 is marked with an X.

inhomogeneous) mesoscale boundaries often increase the tornadic potential of supercells. We might investigate these additional components in future work.

Most of the observed differences between our simulated surface-based and elevated supercells occur in close proximity to the ground. As such, key differences in storm structure that might reveal the tornadic potential of a thunderstorm would typically be well below the scanning horizon of a WSR-88D (Weather Surveillance Radar 88 Doppler). Therefore, nowcasting tornado potential will remain difficult in the short term even with an increased understanding of how near-ground rotation is inhibited in elevated supercells. Nowcasting improvements likely await a better understanding of how much CIN a supercell can encounter and yet remain surface-based, how such thresholds vary as a function of the supercell environment (e.g., vertical wind and buoyancy profiles), and better real-time observations of storm environments.

Acknowledgments. We wish to thank George Bryan for providing the numerical model code as well as Mario Majcen whose advice and code aided our trajectory calculations. Support from NSF grant ATM-0644533 also is acknowledged as well as travel support from the Pennsylvania State University Undergraduate Education Office, College of Earth and Mineral Sciences, and Schreyer Honors College.

REFERENCES

Atkins, N. T., M. L. Weisman, and L. J. Wicker, 1999: The influence of preexisting boundaries on supercell evolution. *Mon. Wea. Rev.*, **127**, 2910–2927.

Bryan, G. H., and J. M. Fritcsh, 2002: A benchmark simulation for moist nonhydrostatic numerical models. *Mon. Wea. Rev.*, **130**, 2917–2928.

Colman, B. R., 1990: Thunderstorms above frontal surfaces in environments without positive CAPE. Part I: A climatology. *Mon. Wea. Rev.*, **118**, 1103–1121.

Davies-Jones, R. P., and H. E. Brooks, 1993: Mesocyclogenesis from a theoretical perspective. *The Tornado: Its Structure, Dynamics, Prediction, and Hazards*, Geophys. Monogr., No. 79, Amer. Geophys. Union, 105-114

Doswell, C. A., D. V. Baker, and C. A. Liles, 2002: Recognition of negative mesoscale factors for severe-weather potential: A case study. *Wea. Forecasting*, **17**, 937–954.

Maddox, R. A., L. R. Hoxit, and C. F. Chappell, 1980: A study of tornadic thunderstorm interactions with thermal boundaries. *Mon. Wea. Rev.*, **108**, 322–336.

Markowski, P. M., E. N. Rasmussen, and J. M. Straka, 1998: The occurrence of tornadoes in supercells interacting with boundaries during VORTEX-95. *Wea. Forecasting*, **13**, 852–859.

Rasmussen, E. N., S. Richardson, J. M. Straka, P. M. Markowski, and D. O. Blanchard, 2000: The association of significant tornadoes with a baroclinic boundary on 2 June 1995. *Mon. Wea. Rev.*, **128**, 174–191.

Rotunno R., and J. B. Klemp, 1982: The influence of the shear-induced pressure gradient on thunderstorm motion. *Mon. Wea. Rev.*, **110**, 136–150.

Rotunno R., and J. B. Klemp, 1985: On the rotation and propagation of simulated supercell thunderstorms. *J. Atmos. Sci.*, **42**, 271–292.

Weisman, M. L., and J. B. Klemp, 1982: The dependence of numerically simulated convective storms on vertical wind shear and buoyancy. *Mon. Wea. Rev.*, **110**, 504–520.